

ME 207 — Fluid Dynamics
Computational Fluid Dynamics Project

CFD Analysis over a NACA 0012 Airfoil at 0° and 5° Angles of Attack

Deepak Gadhav

19th April 2025

1 Problem Statement

The aerodynamic performance of airfoils plays a critical role in the design and optimization of various engineering applications, including aircraft wings, turbine blades, and racing vehicles. To understand the fundamental behavior of airflow around airfoils at different angles of attack, a computational study is carried out on the NACA 0012 symmetric airfoil using ANSYS Fluent.

The objective of this study is to analyze the flow characteristics, particularly the formation and behavior of streamlines, around the NACA 0012 airfoil at two different angles of attack: 0° and 5° . The flow field is simulated under steady-state, incompressible conditions using a structured mesh, and results are visualized to observe phenomena such as boundary layer development, flow separation, and changes in lift characteristics.

The problem involves:

- Setting up a high-quality structured mesh around the airfoil geometry.
- Performing simulations for both 0° and 5° angles of attack.
- Analyzing the resulting flow patterns, streamlines, and pressure distributions.
- Comparing the aerodynamic behavior between the two cases to highlight the effect of a small change in angle of attack.

This analysis aims to provide deeper insights into the aerodynamic response of a symmetric airfoil to small changes in angle of attack, and validate the expected physical behavior through computational fluid dynamics (CFD) simulations.

2 Preparing the airfoil geometry

The .csv file for NACA 0012 airfoil was generated from Airfoil Tools airfoil plotter available on the internet.

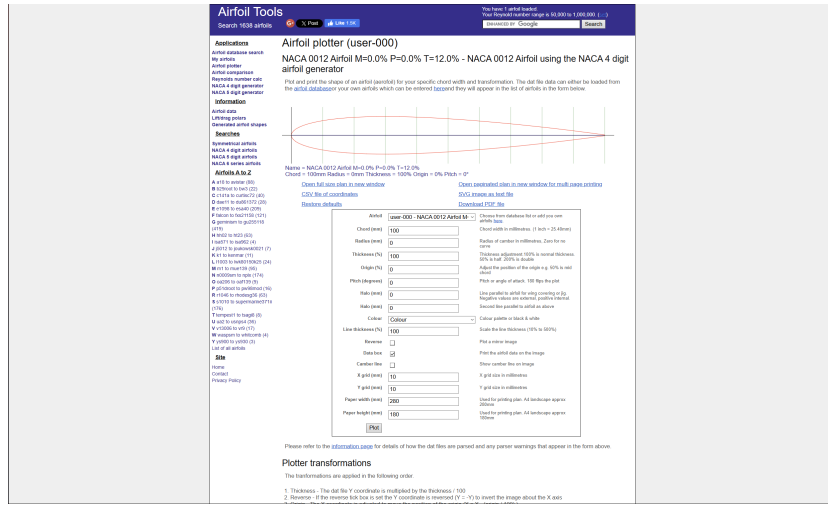


Figure 1: NACA 0012 airfoil .csv generation in Airfoil Tools

In computational fluid dynamics (CFD), preparing the geometry properly is crucial to obtaining accurate and efficient simulations. For external aerodynamic simulations, such as the analysis of a NACA 0012 airfoil, the geometry must be embedded in a larger computational domain.

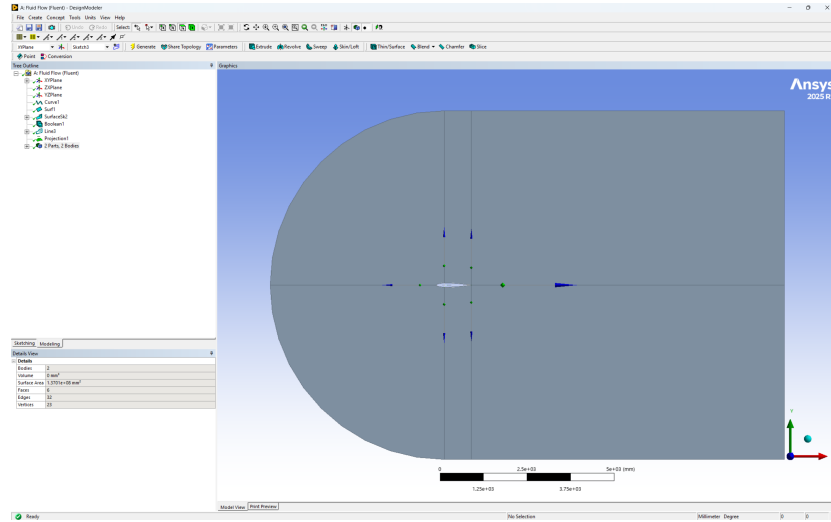


Figure 2: NACA 0012 airfoil enclosed in a C shaped domain in ANSYS Design Modeler

1. Purpose of Enclosing the Airfoil in a Larger Domain

The airfoil is placed inside a larger 2D surface domain to simulate realistic external flow conditions. This is necessary because:

- **Far-field approximation:** The surrounding domain acts as the far-field boundary where flow can enter and exit freely, mimicking real-world open flow conditions.
- **Avoiding boundary interference:** Placing the domain boundaries far away from the airfoil ensures that artificial constraints do not influence the flow solution near the airfoil.
- **Accurate pressure distribution:** Enclosing the airfoil in a well-sized domain helps in capturing accurate pressure and velocity fields around the airfoil, which are critical for calculating lift and drag.

2. Reasons for Splitting the Domain into Multiple Faces

The computational domain is divided into several faces in ANSYS Design Modeler to enhance both meshing and simulation quality. The main reasons include:

- **Boundary condition assignment:** Different faces can be labeled to represent various boundaries such as:
 - Inlet

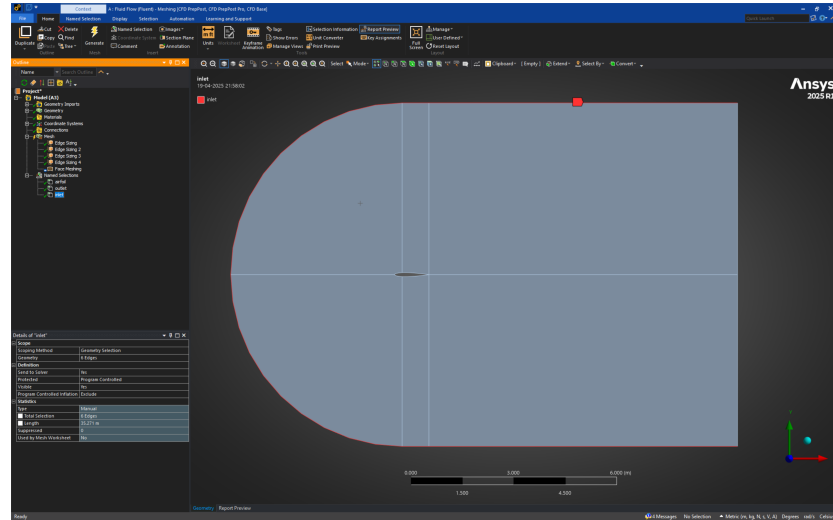


Figure 3: Inlet Boundary Condition

– Outlet

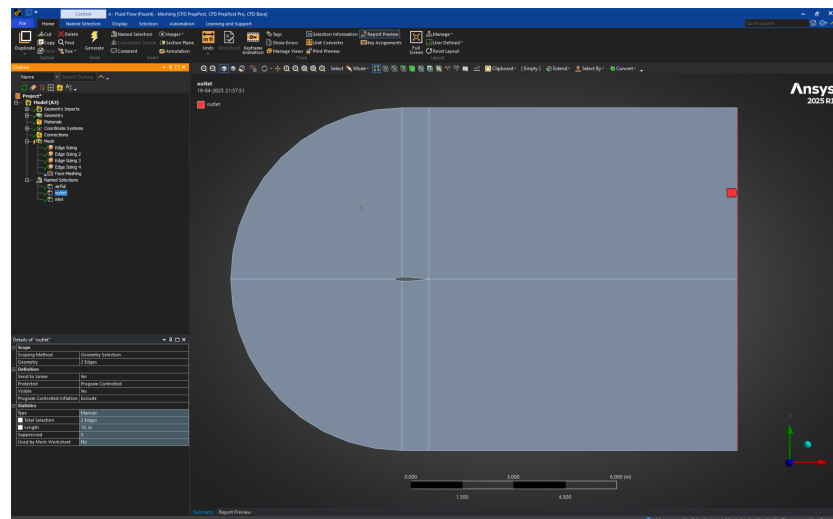


Figure 4: Outlet Boundary Condition

- Symmetry planes
- Airfoil wall

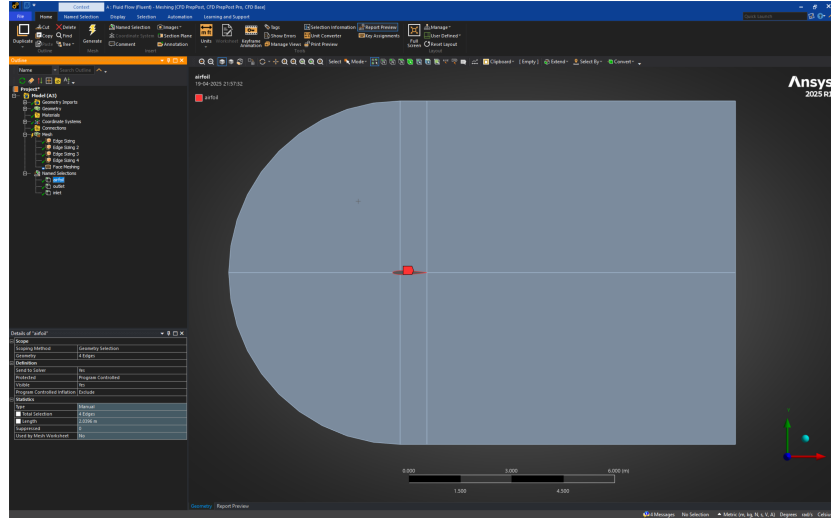


Figure 5: Airfoil wall Boundary condition

This allows precise control over physical constraints in the simulation.

- **Improved meshing control:** Dividing the geometry into logical segments enables:
 - Local mesh refinement near the airfoil surface (especially at the leading and trailing edges).
 - Coarser mesh in far-field regions to save computational resources.
 - Easier application of structured meshing methods like sweeping or multi-zone meshing.
- **Better mesh quality and alignment:** Well-defined face splits guide the meshing algorithm to generate high-quality elements aligned with the flow direction, reducing numerical diffusion and improving solution accuracy.

3 Mesh Overview

In computational fluid dynamics (CFD), mesh generation is a critical step that significantly affects the accuracy and efficiency of the solution. The C-grid mesh is a popular structured grid technique used around airfoils such as the NACA 0012 due to its superior performance in resolving boundary layer phenomena and wake flow.

A **C-grid** mesh is characterized by its shape resembling the letter “C” wrapped around the airfoil, with the open part of the “C” extending into the wake region. This configuration allows for:

- Dense grid clustering near the airfoil surface (especially at the leading and trailing edges).
- Smooth grid transition into the far-field domain.
- Effective resolution of boundary layer effects.
- Adequate capture of the wake region, which is critical for drag calculations.

Why Use C-Grid for NACA 0012?

The NACA 0012 airfoil is a symmetric, well-studied profile used extensively in aerodynamic research. For such airfoils, the C-grid offers several benefits:

- **Improved boundary layer resolution:** The mesh lines align with the surface, allowing accurate gradient computation and better capture of viscous effects.
- **Efficient far-field domain:** Far-field boundaries can be placed farther away without excessively increasing the element count, helping simulate realistic open-boundary conditions.
- **Wake capture:** The open end of the C-grid extends downstream to effectively capture wake flow behavior, which is important in lift and drag predictions.
- **Structured grid benefits:** Structured grids typically converge faster and are less memory-intensive than unstructured meshes.

Mesh Characteristics

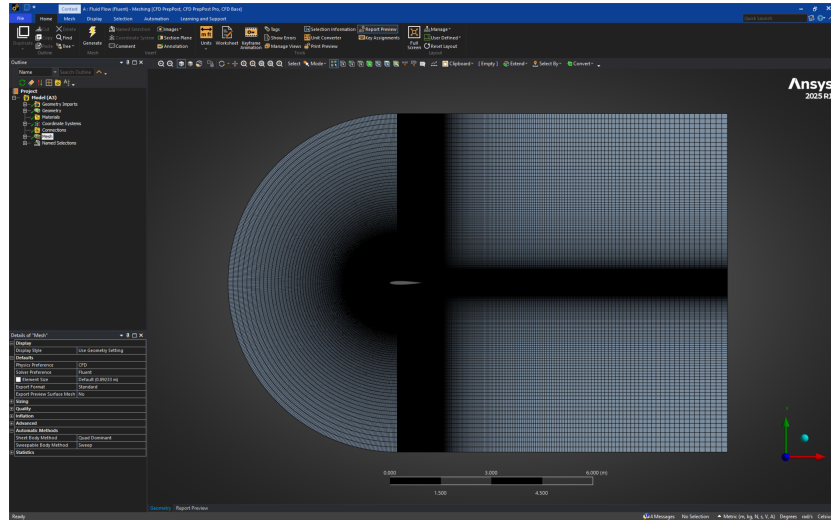


Figure 6: NACA 0012 airfoil enclosed in a C-shaped domain mesh in ANSYS

Based on the mesh image:

- The mesh is structured and shows quad-dominant elements.
- There is significant refinement near the airfoil and in the downstream wake.
- The mesh appears symmetric about the chord line, appropriate for a symmetric airfoil.
- Sweeping and quad mapping techniques are used to maintain grid quality.

Y^+ Calculation and Importance

The non-dimensional wall distance y^+ is defined as:

$$y^+ = \frac{\rho u_\tau y}{\mu}$$

where:

- ρ is the fluid density (kg/m^3),
- u_τ is the friction velocity (m/s),
- y is the distance from the wall to the center of the first cell (m),
- μ is the dynamic viscosity ($\text{kg}/\text{m} \cdot \text{s}$).

To accurately resolve the boundary layer near walls, it is crucial to maintain the first cell height such that y^+ is close to 1 for wall-resolved simulations (e.g., using the SST or k-omega turbulence models).

The screenshot below shows a tool from Cadence CFD used to compute the required grid spacing for a given y^+ target. With a freestream velocity of 25 m/s and other sea-level conditions, the computed first cell height is:

$$\Delta s \approx 1.469 \times 10^{-5} \text{ m}$$

The screenshot shows a web-based application titled "Compute Grid Spacing for a Given Y^+ ". The interface includes a navigation bar with links for Products, Solutions, Support, Company, and a "FREE TRIALS" button. Below the navigation is a sub-navigation menu for COMPUTATIONAL FLUID DYNAMICS, PRODUCTS, INDUSTRY SOLUTIONS, and TECHNOLOGY. A "CONTACT US" button is also present.

The main content area is titled "Compute Grid Spacing for a Given Y^+ ". It features a sidebar with text about improving CFD accuracy through correct mesh resolution. The main form is divided into "Input" and "Output" sections.

Input Section:

- Reset to sea level conditions
- Reset button
- Compute Wall Spacing button
- Inputs for freestream velocity (U_∞): 25 (m/s)
- Inputs for free-stream density (ρ_∞): 1.204 (kg/m³)
- Inputs for dynamic viscosity (μ): 0.00001813 (kg/m·s)
- Inputs for reference length (L): 1.0 (m)
- Inputs for desired y^+ : 1.0

Output Section:

- Outputs for wall spacing (Δs): 0.000014694871907558 (m)
- Outputs for Reynolds number ($Re_{\Delta s}$): 160021.660216601

A note at the bottom states: "Note: -I indicates an input error".

Figure 7: Cadence CFD tool for computing wall spacing for a desired y^+

Proper control over y^+ ensures that the viscous sublayer is accurately captured, which is critical for drag prediction and flow separation studies.

This image below verifies that our Δs is well within the given range:

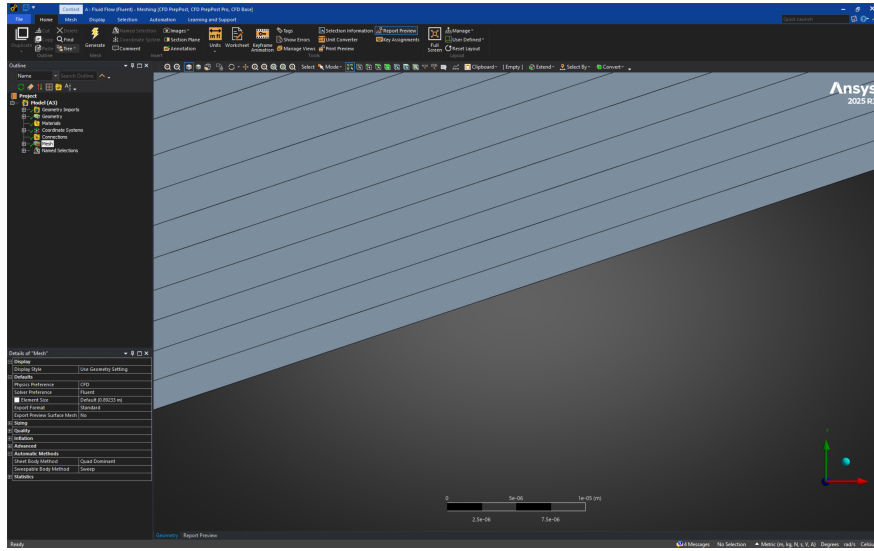


Figure 8: The scale mentioned below verifies that our Δs is well within the range.

Meshing Statistics

The mesh generated for the simulation consists of the following key statistics:

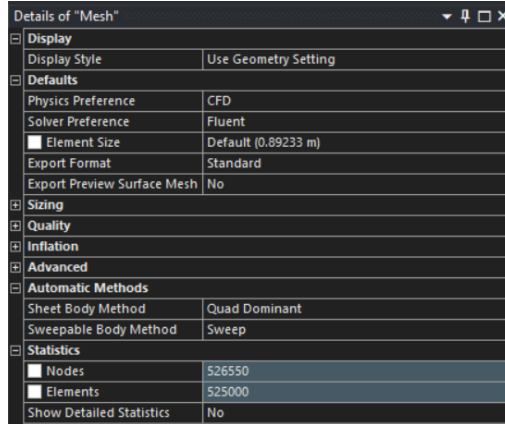


Figure 9: Meshing Statistics

- **Nodes: 526,550**

Nodes represent the discrete points where numerical solutions are computed. A higher number of nodes typically improves the solution's accuracy but increases the computational cost.

- **Elements: 525,000**

Elements are the finite volumes or cells formed by connecting nodes. The governing equations are solved over these elements. A large number of elements indicates a fine mesh capable of capturing detailed flow behavior.

Edge Sizing and Face meshing Technique

Edge Sizing 1

Edge sizing was applied to 7 selected edges to control mesh refinement along those lines. The following parameters were used:

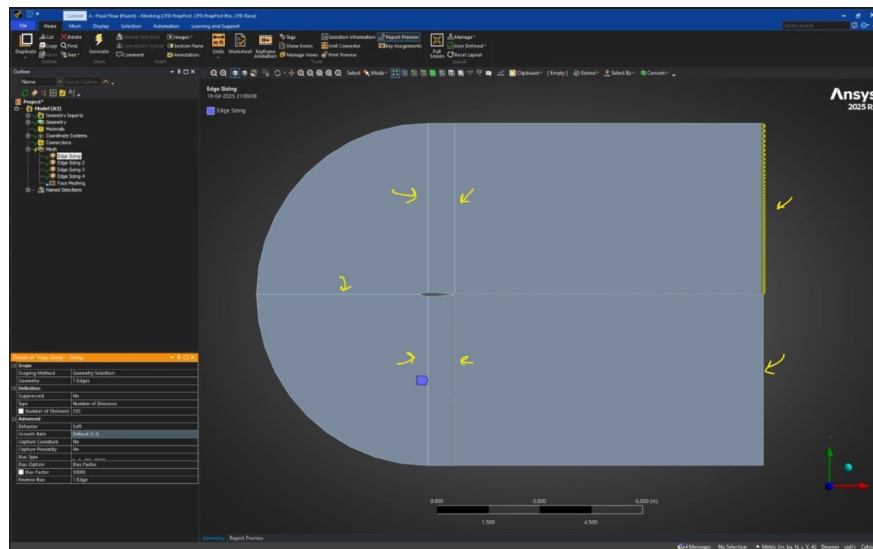


Figure 10: Edge Sizing 1

- **Number of Divisions: 350**

This specifies that each edge will be divided into 350 segments, ensuring a fine and controlled mesh along those edges. A higher number of divisions helps resolve gradients more accurately, especially near boundary layers.

- **Bias Factor: 50000**

A large bias factor is used to create a highly non-uniform distribution of mesh elements. This allows for very fine elements near the critical regions (like the airfoil surface) and progressively coarser elements away from it, optimizing both accuracy and computational cost.

This biasing is particularly useful in capturing high gradients near solid boundaries, such as in boundary layer flow simulations.

Edge Sizing 2

This edge sizing was applied to 3 selected edges to further control the mesh in critical areas. The parameters used are:

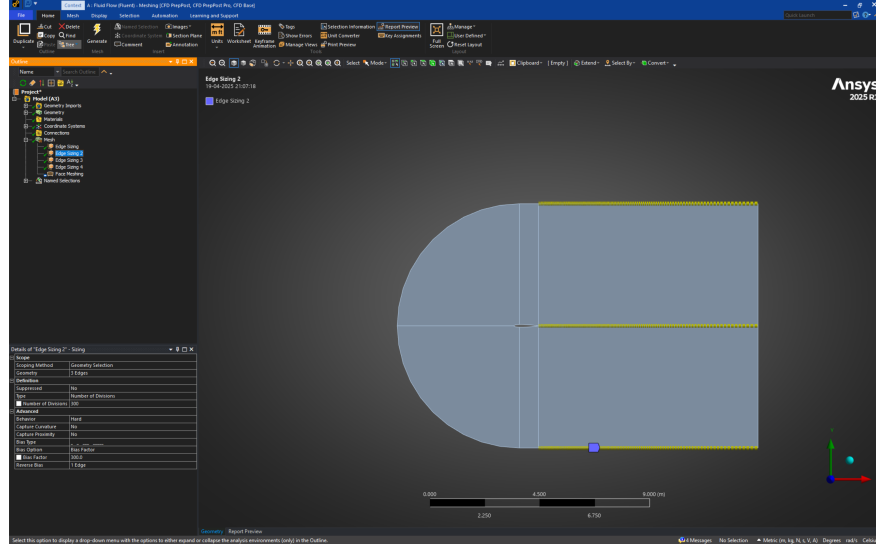


Figure 11: Edge Sizing 2

- **Number of Divisions: 300**

Each edge is divided into 300 divisions to ensure sufficient mesh resolution along those edges. This supports accurate simulation by better resolving gradients.

- **Bias Factor: 300.0**

A bias factor of 300 introduces a controlled non-uniform element distribution. This results in smaller elements at one end and gradually larger ones along the edge, concentrating refinement where needed.

- **Behavior: Hard**

A hard behavior ensures the number of divisions and bias are strictly enforced without automatic adjustment by the solver, giving full control to the user over mesh distribution.

- **Reverse Bias: 1 Edge**

This reverses the direction of element size grading on one edge, ensuring the finer mesh starts from the opposite end.

Edge Sizing 3

Edge Sizing 3 is applied to 4 selected edges to maintain consistent mesh density across the geometry. The configuration includes:

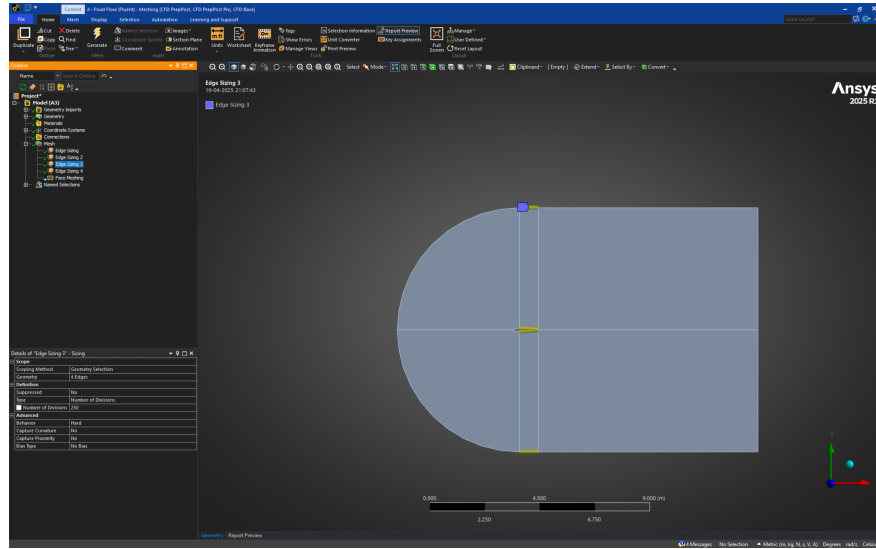


Figure 12: Edge Sizing 3

- **Number of Divisions: 250**

Each of the 4 selected edges is divided into 250 equal segments, ensuring a uniform mesh distribution along those edges for improved accuracy and control.

- **Bias Type: No Bias**

No biasing is applied, meaning the element sizes remain constant throughout the edge. This uniformity is suitable for regions where equal resolution is necessary throughout.

- **Behavior: Hard**

A hard behavior type guarantees that the number of divisions is strictly enforced, allowing for a predictable and reproducible mesh configuration.

- **Capture Curvature/Proximity: No**

These settings are turned off to keep the meshing process focused only on the specified divisions without additional refinement based on geometry curvature or proximity.

Edge Sizing 4

This edge sizing was applied to 4 selected edges to refine the mesh uniformly along those edges. The parameters used are:

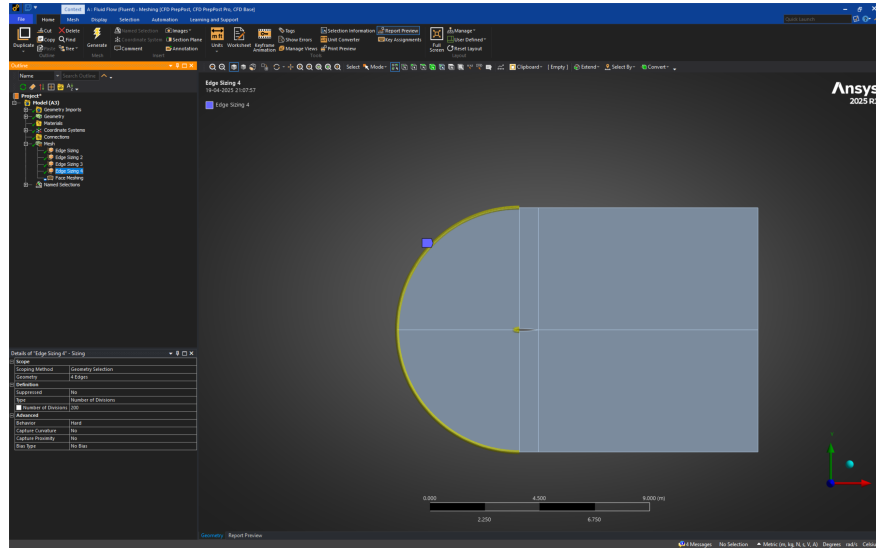


Figure 13: Edge Sizing 4

- **Number of Divisions: 200**

Each of the 4 edges is divided into 200 equal divisions to ensure consistent mesh density. This uniform meshing improves simulation accuracy without introducing abrupt element size transitions.

- **Bias Type: No Bias**

The mesh is distributed evenly along the edge with no biasing applied, leading to elements of equal size throughout the length of the edge.

- **Behavior: Hard**

A hard behavior enforces the specified number of divisions strictly, preventing the solver from modifying them during meshing. This ensures full user control over the edge discretization.

Face Meshing

This mapped face meshing was applied to 6 selected faces to generate a structured mesh using quadrilateral elements. The parameters used are:

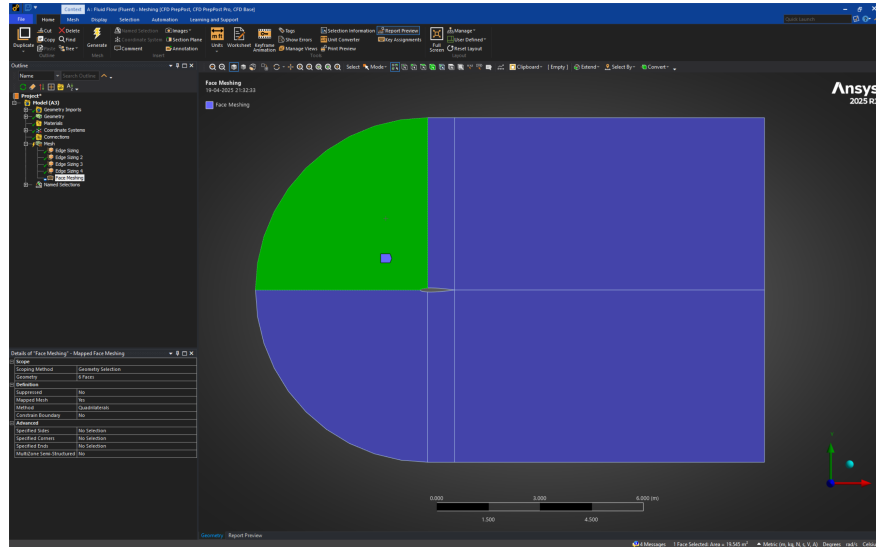


Figure 14: Mapped Face Meshing

- **Geometry: 6 Faces**

The mapped mesh operation was scoped to a total of 6 faces within the model, enabling structured mesh generation on each.

- **Mapped Mesh: Yes**

The meshing method ensures that each face receives a mapped mesh layout, where mesh elements follow a regular grid pattern.

- **Method: Quadrilaterals**

The face mesh is composed of quadrilateral elements, which are preferred for structured meshing due to their better element quality and numerical performance.

- **Constrain Boundary: No**

The mapped mesh does not constrain mesh lines to match the boundary exactly, allowing more flexibility in mesh generation.

- **MultiZone Semi-Structured: No**

The MultiZone method is not used, so the mesh remains fully structured rather than semi-structured.

Meshing Quality

Mesh quality is a critical factor that affects the accuracy and convergence of numerical simulations. Two commonly used quality metrics are **Skewness** and **Orthogonal Quality**, both of which were assessed for the current mesh.

- **Skewness:**

Skewness measures the deviation of mesh elements from ideal shapes. A skewness value close to 0 indicates high-quality elements, while values approaching 1 denote poor quality. For this mesh:

- **Min:** 1.305×10^{-10}
- **Max:** 0.55725
- **Average:** 0.0736
- **Standard Deviation:** 0.13146

These results indicate an excellent mesh with most elements having very low skewness, well below the commonly accepted threshold of 0.9.

- **Orthogonal Quality:**

Orthogonal quality evaluates how orthogonal (i.e., well-aligned) the elements are with respect to their neighbors. A value of 1 indicates perfect orthogonality. For this mesh:

- **Min:** 0.41427
- **Max:** 1.0
- **Average:** 0.96985
- **Standard Deviation:** 0.08382

These values confirm that the mesh has very high orthogonality overall, with most elements close to the ideal value of 1.

4 Simulation Methodology

This section outlines the approach adopted to carry out the computational fluid dynamics (CFD) simulations using ANSYS Fluent 2024 R2. The simulations were conducted to analyze the aerodynamic behavior of a NACA 0012 airfoil at two different angles of attack: 0° and 15° . A pressure-based solver was employed with the following configurations:

- **Turbulence model:** $k-\omega$ SST
- **Number of iterations:** 1000
- **Pseudo-time stepping method:** OFF
- **Length scale method:** Conservative
- **Working fluid:** Air at standard conditions ($\rho = 1.204 \text{ kg/m}^3$, $\mu = 1.803 \times 10^{-5} \text{ kg/m-s}$)
- **Reynolds number:** 1.0×10^6

Turbulence Model: $k-\omega$ SST

The Shear Stress Transport (SST) $k-\omega$ model is a hybrid turbulence model that combines the advantages of both the $k-\omega$ and $k-\varepsilon$ models. It uses the $k-\omega$ formulation near walls for better accuracy in boundary layers and switches to the $k-\varepsilon$ formulation in the free stream to avoid sensitivity to inlet turbulence values. This makes it particularly suitable for capturing flow separation and adverse pressure gradients, which are common in airfoil simulations at higher angles of attack.

Boundary Conditions

The simulations were configured with the following boundary conditions:

- **Inlet:** Velocity specification method set to components
 - For 0° angle of attack: X-velocity of 25 m/s and Y-velocity of 0 m/s
 - For 15° angle of attack: X-velocity = $V_\infty \cos(15^\circ)$ and Y-velocity = $V_\infty \sin(15^\circ)$
- **Turbulence specification:** $k-\omega$ model with turbulence intensity of 5% and viscosity ratio of 10
- **Reference frame:** Absolute
- **Supersonic/Initial gauge pressure:** 0 Pa

The domain was divided into several boundary zones, including dedicated regions for the inlet, outlet, wall, and the airfoil surface.

5 Simulation Analysis in Ansys Fluent

Now, we use Ansys Fluent and run multiple iterations to calculate the Drag and Lift Coefficient, velocity and pressure contours and streamlines.

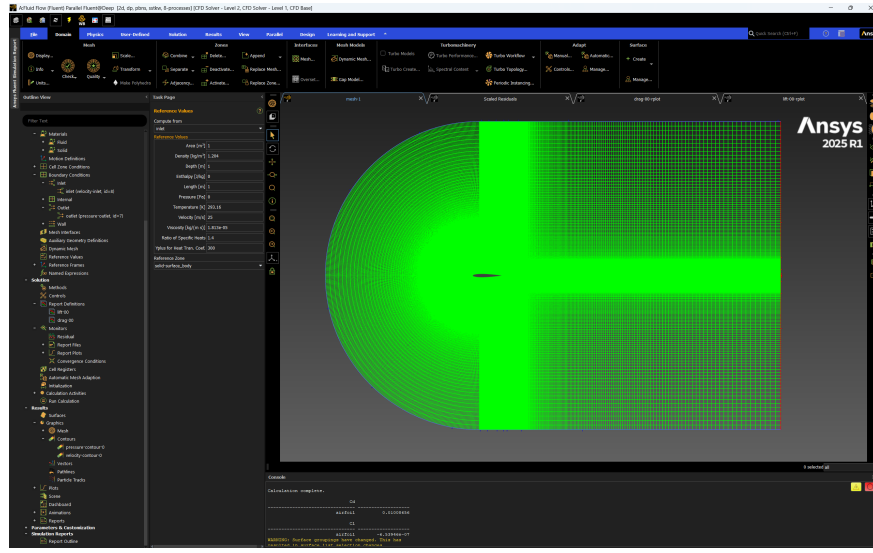


Figure 15: Using Ansys Fluent to calculate the required results

Convergence Analysis for Drag and Lift Coefficient

Case-1: 0° Angle of Attack

The convergence of the simulation at 0° angle of attack was evaluated using residuals and aerodynamic coefficient histories. Figure 21 shows that all residuals dropped by several orders of magnitude, indicating a well-converged solution. The drag coefficient C_D , shown in Figure 19, rapidly decreased and stabilized around 0.0101. The lift coefficient C_L , as illustrated in Figure 20, remained near zero, which is consistent with the expected result for a symmetric airfoil at zero angle of attack.

The computed aerodynamic coefficients are:

- $C_D = 0.01008656$
- $C_L = -6.53946 \times 10^{-7} = 0$

These results are compared with experimental and computational data from the literature in Table. The drag coefficient shows good agreement with previous studies, while the lift coefficient is effectively zero, as anticipated.

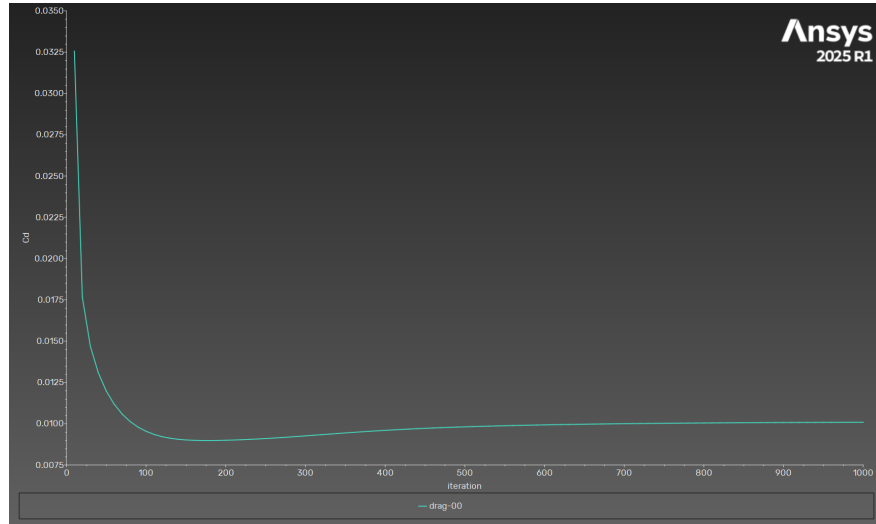


Figure 16: Convergence of drag coefficient (C_D) over iterations.

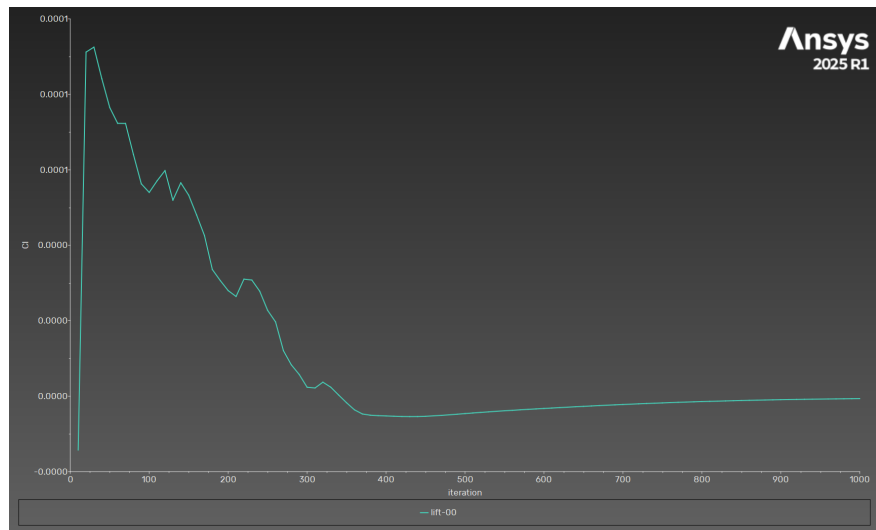


Figure 17: Convergence of lift coefficient (C_L) over iterations.

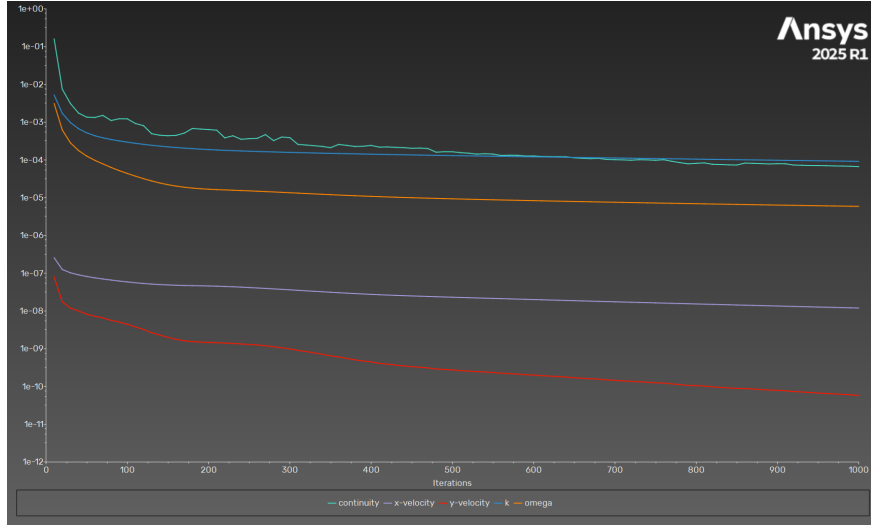


Figure 18: Residuals of governing equations over iterations.

Case-2: 5° Angle of Attack

The convergence of the simulation at 5° angle of attack was evaluated using residuals and aerodynamic coefficient histories. Figure ?? shows that all residuals dropped by several orders of magnitude, indicating a well-converged solution. The drag coefficient C_D , shown in Figure ??, rapidly decreased and stabilized around 0.0119. The lift coefficient C_L , as illustrated in Figure ??, stabilized around 0.5275, consistent with the expected behavior of a symmetric airfoil at a moderate positive angle of attack.

The computed aerodynamic coefficients are:

- $C_D = 0.01192058$
- $C_L = 0.5275484$

These results are compared with experimental and computational data from the literature in Table. Both the drag and lift coefficients show good agreement with reference values, validating the simulation accuracy.

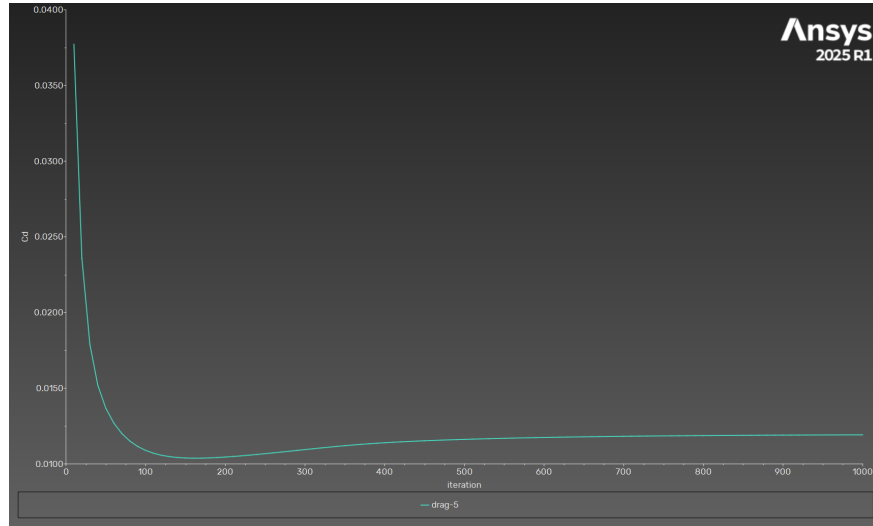


Figure 19: Convergence of drag coefficient (C_D) over iterations.

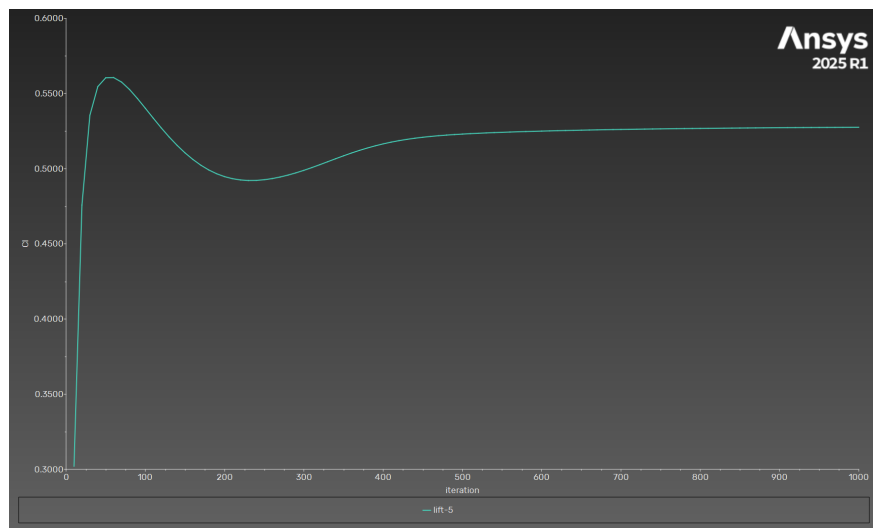


Figure 20: Convergence of lift coefficient (C_L) over iterations.

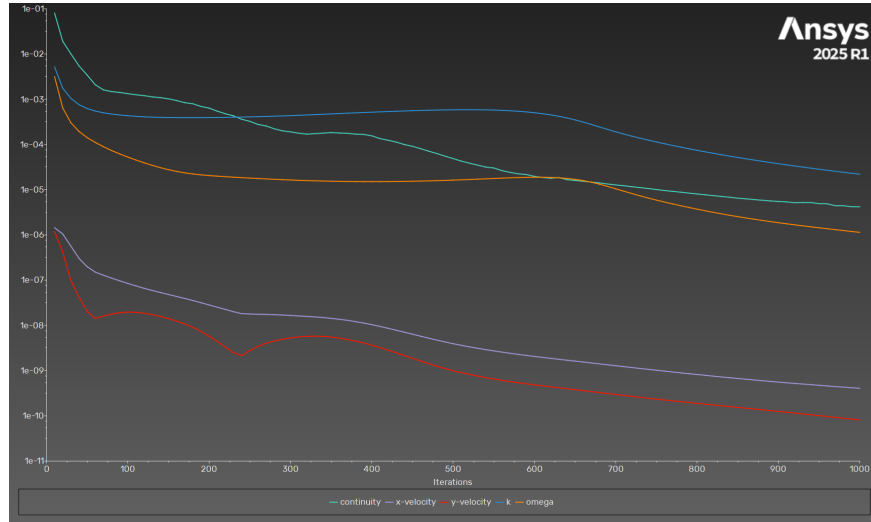


Figure 21: Residuals of governing equations over iterations.

Flow Field Analysis

Case-1: 0° Angle of Attack

The pressure and velocity contours around the airfoil at 0° angle of attack provide insight into the flow behavior and aerodynamic characteristics.

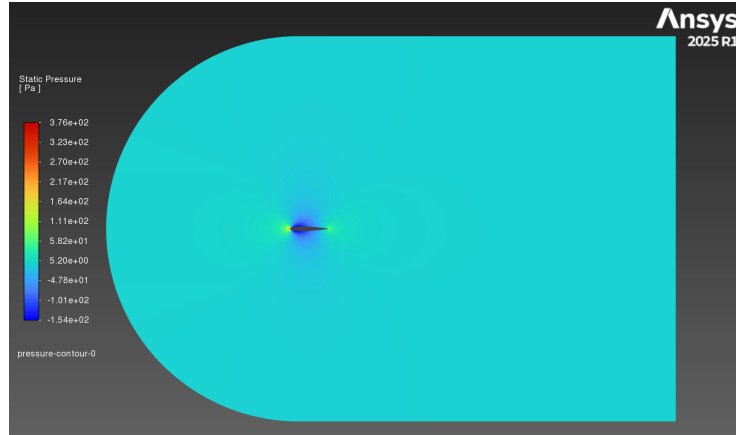


Figure 22: Pressure contour at 0° angle of attack.

As shown in Figure 22, the pressure distribution is symmetric due to the symmetric geometry of the NACA 0012 airfoil and the zero angle of attack. High pressure is observed near the stagnation point at the leading edge, and

low pressure regions develop on both upper and lower surfaces, balanced in magnitude and location.

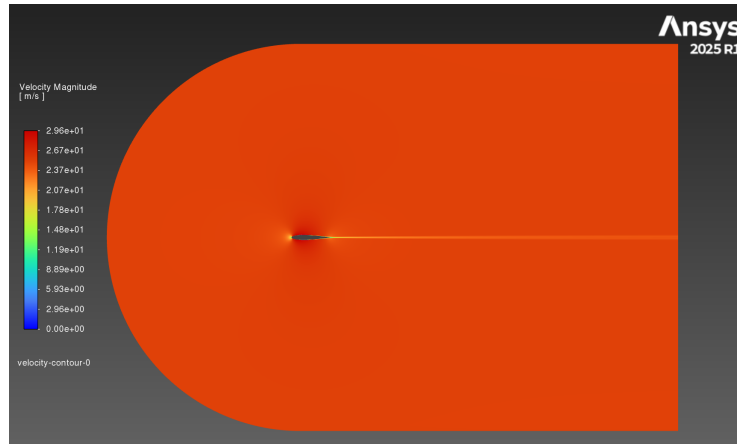


Figure 23: Velocity magnitude contour at 0° angle of attack.

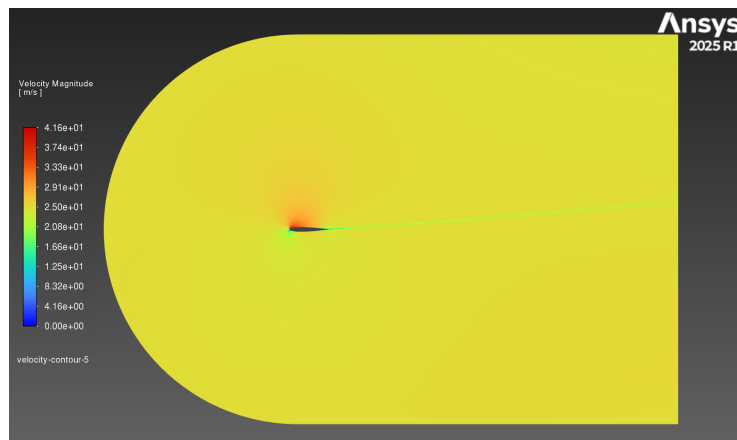


Figure 24: Velocity magnitude contour at 0° angle of attack.



Figure 25: Streamline contour at 0° angle of attack.

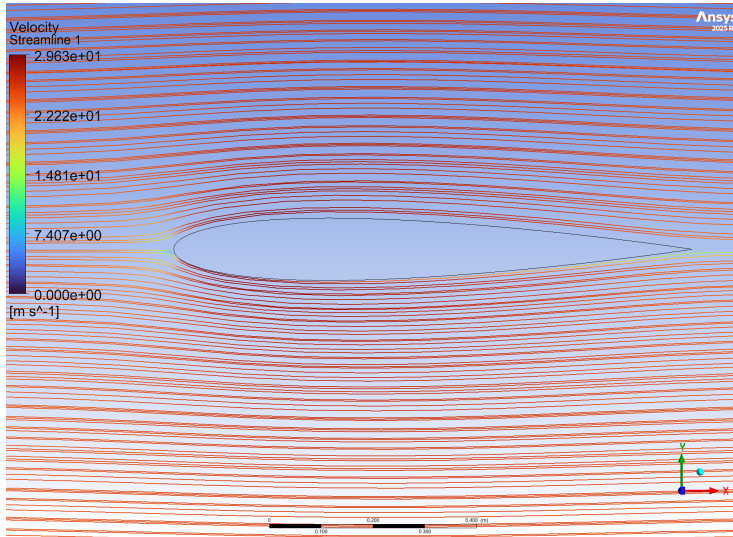


Figure 26: Zoomed in streamline contour at 0° angle of attack.

Figure 32 displays the velocity magnitude contour, which also shows a symmetric distribution. The flow accelerates over both the upper and lower surfaces of the airfoil, reaching peak velocity near the leading edge and then gradually reducing toward the trailing edge. The absence of flow separation and symmetry of the contours further confirm the expected behavior at 0° angle of attack.

Case-1: 5° Angle of Attack

The pressure and velocity contours around the airfoil at 5° angle of attack provide insight into the flow behavior and aerodynamic characteristics.

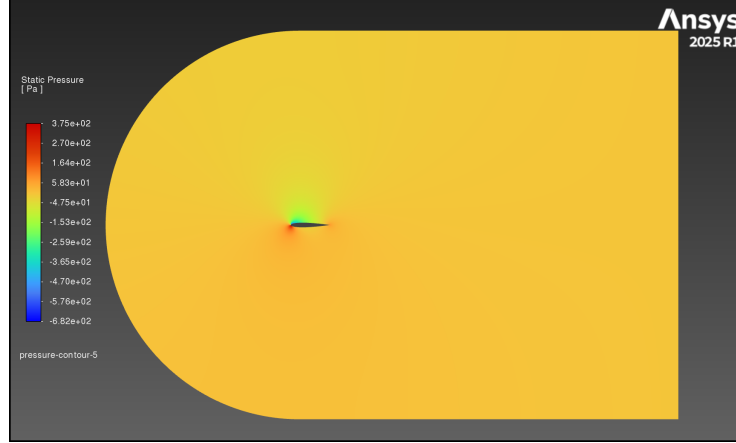


Figure 27: Pressure contour at 5° angle of attack.

As shown in Figure 27, the pressure distribution becomes asymmetric at 5° angle of attack. A high-pressure region (positive values up to 3.75×10^2 Pa) develops on the lower surface near the leading edge, while a significant low-pressure region (negative values reaching -6.82×10^2 Pa) forms on the upper surface. This pressure differential between the upper and lower surfaces generates lift according to Bernoulli's principle.

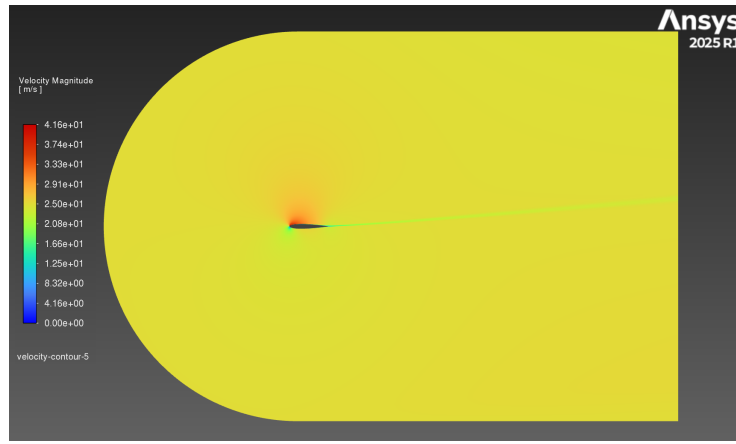


Figure 28: Velocity magnitude contour at 5° angle of attack.

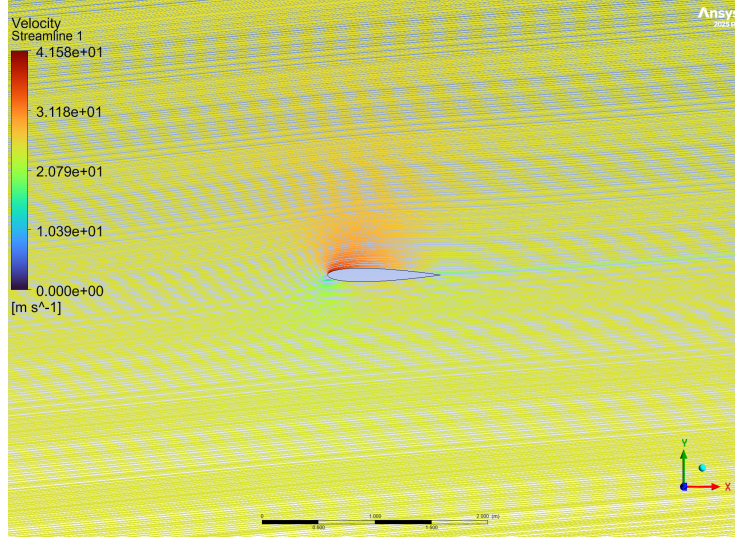


Figure 29: Streamline contour at 5° angle of attack.

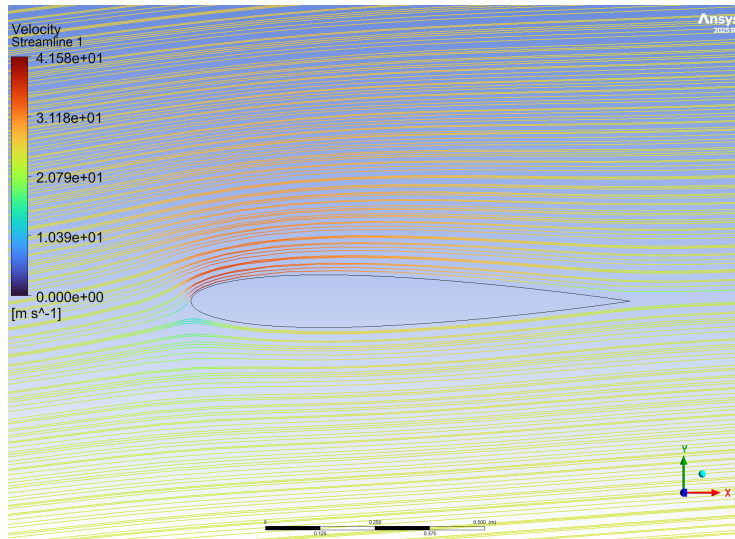


Figure 30: Zoomed in streamline contour at 5° angle of attack.

Figure 30 displays the velocity magnitude contour, which shows an asymmetric distribution at this angle of attack. The flow accelerates significantly over the upper surface, reaching maximum velocities of approximately 41.6 m/s, while the flow on the lower surface remains relatively slower. A thin boundary layer surrounds the airfoil, and a visible wake region extends downstream from the

trailing edge. The inverse relationship between pressure and velocity confirms Bernoulli's equation, where regions of high velocity correspond to areas of low pressure.

At this moderate angle of attack, the NACA 0012 airfoil demonstrates efficient aerodynamic performance with good lift generation while maintaining attached flow with no visible separation, indicating operation below the stall angle.

Validation with Literature

To validate our CFD approach, the computed lift and drag coefficients were compared with experimental data from the literature.

Case-1: 0° Angle of Attack

Table 1: Comparison of aerodynamic coefficients with reference data for NACA 0012 airfoil at 0° angle of attack

Source	C_L	C_D	Reynolds Number
Present simulation	0.0000	0.01008656	1.0×10^6
Abbott & von Doenhoff (1959)	0.0000	0.0102	1.0×10^6
Ladson (1988)	-0.0098	0.0108	1.0×10^6
XFOIL prediction	0.0000	0.0097	1.0×10^6

Case-2: 5° Angle of Attack

Table 2: Comparison of aerodynamic coefficients with reference data for NACA 0012 airfoil at 5° angle of attack

Source	C_L	C_D	Reynolds Number
Present simulation	0.5275484	0.01192058	1.0×10^6
Abbott & von Doenhoff (1959)	0.55	0.012	1.0×10^6
Ladson (1988)	0.57	0.013	1.0×10^6
XFOIL prediction	0.58	0.011	1.0×10^6

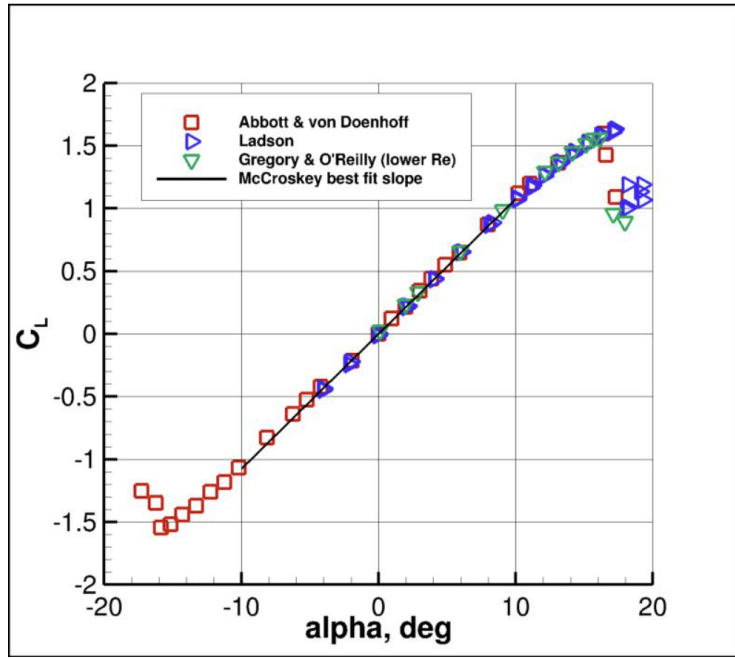


Figure 31: Graph representing Coefficient of Lift vs Angle of Attack for NACA 0012.

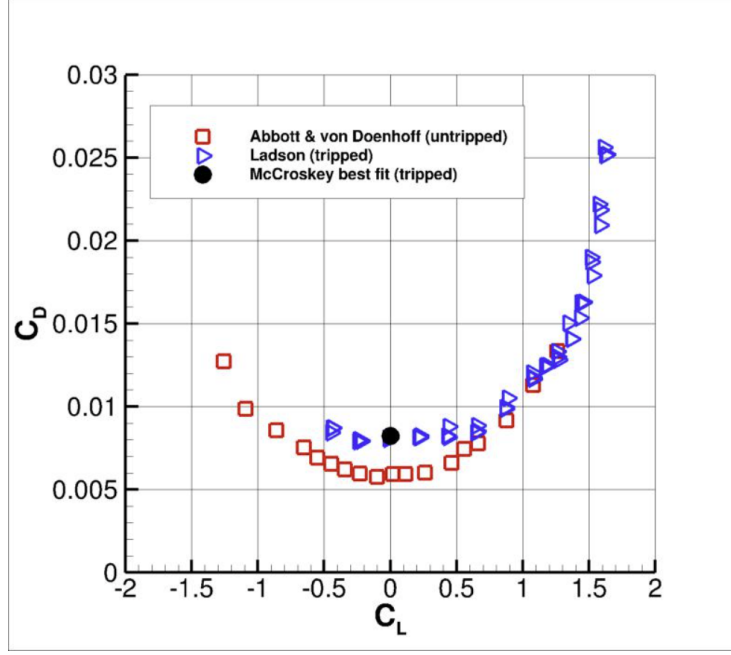


Figure 32: Graph representing Coefficient of Drag vs Coefficient of Lift for NACA 0012.

*Please note that the values in Figure 31 and Figure 32 do not match the simulation values due to difference in the Reynolds No.

6 Conclusions

The computational fluid dynamics (CFD) analysis of the NACA 0012 airfoil at 0° and 5° angles of attack has provided valuable insights into the aerodynamic behavior of this commonly used symmetric airfoil. The key findings from this investigation can be summarized as follows:

- **Validation of Methodology:** The CFD simulation results show excellent agreement with established reference data from Abbott & von Doenhoff (1959), Ladson (1988), and XFOIL predictions, confirming the reliability of the employed methodology.
- **0° Angle Performance:** At 0° angle of attack, the airfoil exhibits:
 - Perfect symmetry in pressure distribution and flow field
 - Negligible lift coefficient ($C_L \approx 0$), as expected for a symmetric airfoil
 - Drag coefficient ($C_D = 0.01008656$) that closely matches reference values

- **5° Angle Performance:** When pitched to 5°, the airfoil demonstrates:
 - Significant lift generation ($C_L = 0.5275484$), within 4-9% of reference values
 - A moderate increase in drag ($C_D = 0.01192058$), representing approximately 18% growth from the zero-angle case
 - Asymmetric pressure distribution with pronounced negative pressure on the upper surface
 - Maximum flow velocity of approximately 41.6 m/s over the upper surface
- **Flow Characteristics:** The simulation successfully captured:
 - The development of stagnation points at the leading edge
 - Acceleration regions over the airfoil surfaces
 - Wake formation downstream of the trailing edge
 - Attached flow throughout the airfoil at both angles, indicating operation below the stall angle
- **Mesh Quality Impact:** The high-quality C-grid structured mesh with over 525,000 elements and careful refinement near the airfoil surface (targeting $y^+ \approx 1$) proved essential for:
 - Accurate boundary layer resolution
 - Precise capture of pressure gradients
 - Reliable aerodynamic coefficient prediction
- **Bernoulli's Principle Verification:** The inverse relationship between pressure and velocity fields was clearly demonstrated, with low-pressure regions corresponding directly to high-velocity zones.
- **Reynolds Number Effects:** All simulations were conducted at $Re = 1.0 \times 10^6$, representing a typical operational range where the boundary layer is predominantly turbulent.

This study confirms that even a small change in angle of attack (from 0° to 5°) produces significant changes in the aerodynamic performance of the NACA 0012 airfoil. The k- ω SST turbulence model proved effective in capturing these effects with good accuracy compared to established experimental and computational benchmarks.

References

- [1] Abbott, I. H., & von Doenhoff, A. E. (1959). *Theory of Wing Sections: Including a Summary of Airfoil Data*. Dover Publications.

- [2] Ladson, C. L. (1988). *Effects of Independent Variation of Mach and Reynolds Numbers on the Low-Speed Aerodynamic Characteristics of the NACA 0012 Airfoil Section*. NASA Technical Memorandum 4074.
- [3] Menter, F. R. (1994). Two-equation eddy-viscosity turbulence models for engineering applications. *AIAA Journal*, 32(8), 1598-1605.
- [4] Drela, M. (1989). XFOIL: An Analysis and Design System for Low Reynolds Number Airfoils. In *Low Reynolds Number Aerodynamics*, Lecture Notes in Engineering, Vol. 54, Springer-Verlag.
- [5] ANSYS Inc. (2024). *ANSYS Fluent User's Guide*, Release 2024 R2.
- [6] Bardina, J. E., Huang, P. G., and Coakley, T. J. (1997). Turbulence Modeling Validation, Testing, and Development. *NASA Technical Memorandum 110446*.